Blood First Edition Paper, prepublished online December 14, 2006; DOI 10.1182/blood-2005-11-056689

THE β-TAIL DOMAIN (βTD) REGULATES PHYSIOLOGIC LIGAND BINDING TO INTEGRIN CD11b/CD18

Vineet Gupta, Annette Gylling, Jose-Louis Alonso, Takashi Sugimori, Petre Ianakiev, Jiang-Ping Xiong and M. Amin Arnaout*

Nephrology Division, Leukocyte Biology & Inflammation Program, Structural Biology Program, Massachusetts General Hospital, Harvard Medical School, Charlestown, MA, 02129

Running Title: The βTD regulates integrin CD11b/CD18

* Correspondence should be addressed to: M. Amin Arnaout,
E-Mail: arnaout@receptor.mgh.harvard.edu
Tel. 617-726-5663
Fax: 617-726-5671

Abstract

Crystallographic and electron microscopy studies revealed genuflexed (bent) integrins in both unliganded (inactive) and physiologic ligand-bound (active) states, suggesting that local conformational changes are sufficient for activation. Herein we have explored the role of local changes in the contact region between the membrane-proximal β–tail domain (βTD) and the ligand-binding βA domain of the bent conformation, in regulating interaction of integrin CD11b/CD18 (αMβ2) with its physiologic ligand iC3b. We replaced the βTD CD loop residues D658GMD of the CD18 (β2) subunit with the equivalent D672SSG of the β3 subunit, with AGAA or with NGTD, expressed the respective heterodimeric receptors either transiently in epithelial HEK293T cells or stably in leukocytes (K562), and measured their ability to bind iC3b and to conformation-sensitive mAbs. In the presence of the physiologic divalent cations Ca^{2+} plus Mg^{2+} (at 1mM each), the modified integrins showed increased (in HEK293) or constitutive (in K562) binding to iC3b, compared to wild-type receptors. K562 expressing the βTD-modified integrins bound in Ca^{2+}/Mg^{2+} to the βA-directed high-affinity reporter mAb 24 but not to mAb KIM127, a reporter of the genu-straightened state. These data identify a role for the membrane proximal βTD as an allosteric modulator of integrin activation.

Introduction

Integrins are αβ heterodimeric receptors normally expressed in an inactive state on the cell surface but can switch rapidly and reversibly to the active physiologic ligand binding state, in response to inside-out activation signals generated from within cells (reviewed in [1]). The integrin ectodomain consists of a "head" segment on top of two "leg" segments [2,3] (Figure 1). The head segment is formed of a seven-bladed β-propeller from the α-subunit that associates noncovalently with a von Willebrand factor type A (vWFA) domain (βA or I-like) from the β-subunit. The α-subunit leg is formed of an Ig-like "thigh" domain followed by two large β-sandwich domains, calf-1 and calf-2. The β-subunit leg is formed of an Ig-like "hybrid" domain inserted into the n-terminal PSI domain [4,5], followed by four EGF-like domains and a novel beta tail domain (βTD) [2](Figure 1). In native integrins, each leg terminates in a single membrane-spanning segment and a short cytoplasmic tail. The prototypical ligand Arg-Gly-Asp binds to the head segment such that the ligand aspartate engages βA through a metal ion coordinated at the *m*etal-*i*on-*d*ependent-*a*dhesion *s*ite (MIDAS) and the ligand arginine fits an adjacent pocket in the propeller [3]. One-half of the integrin α-subunits have an additional vWFA domain (αA or I), inserted between blades 2 and 3 of the propeller. αA exists in inactive and active conformations, and the α1 helix, the βF-α7 (F/α7) loop and α7 helix are known to be involved in this transition [6-8]. In the active conformation of αA-containing integrins, a c-terminal glutamate from active αA ligates the βA MIDAS, stabilizing the high affinity state [9].

Integrins assume a compact conformation, bent at its αβ "knees" -these are located between the thigh and calf-1 domains of the α-subunit and presumably EGF1 and EGF2 of the β-subunit- such that the head contacts the lower legs of the same molecule [2]. Earlier electromicroscopy (EM) images showing genu-straightened integrins [10] led to the early suggestion that inside-out activation (induction of physiologic ligand-competency) takes place as a result of a switch from the bent to the linear state [11]. Additional studies have shown, however, that such as global change is not required for switching to high binding affinity [12-15], suggesting that local changes may be sufficient to enable physiologic ligand-binding in the bent state (reviewed in [16]). In the crystal structure of the unliganded αVβ3 ectodomain [2], the βA and hybrid domains make discontinuous intramolecular contacts with the βTD, covering a combined ~334 Å of surface area. In this communication, we have examined the role of βTD's CD loop, which contacts βA, in physiologic ligand binding to integrin CD11b/CD18. The results reveal an important allosteric function for the βTD in regulating physiologic ligand binding by this integrin.

Materials and Methods

Reagents and Antibodies. Restriction and modification enzymes were obtained from New England Biolabs Inc. (Beverly, MA), GIBCO BRL (Gaithersburg, MD) or Fisher Scientific. All cell culture reagents were from Invitrogen Corp. (San Diego, CA). The anti-CD11b monoclonal antibody (mAb) 44a (IgG2a) [17], the anti-CD18 mAb TS1/18 [18], the heterodimer-specific mAb IB4 (IgG2a)[19,20], and a polyclonal anti-CD18 antibody [21] have been described previously. Monoclonal antibodies KIM127 and 24 (both IgG1) were kindly provided by M. Robinson [22] and N. Hogg [23] respectively. Isotype control antibodies MOPC-21 (IgG1) and MOPC-173 (IgG2a), FITC-conjugated mAbs A85-1 (rat anti-mouse IgG1), R19-15 (rat anti-mouse IgG2a) and goat anti-mouse Ig were from BD Pharmingen (San Diego, CA).

DNA Constructs. Site-directed CD18 mutants were created using standard recombinant DNA protocols [24] in pcDNA3 expression vectors [25]. The following forward (For) and reverse (Rev) oligonucleotides were used, each followed by the newly introduced restriction site in brackets:
For:5'-CACGCTGGAGCAGCAGGACtcGtccGgCCGCTACCTCATCTATGTGGATG-3' *(Eag*);
Rev:5'-CATCCACATAGATGAGGTAGCGGcCggaCgaGTCCTGCTGCTCCAGCGTG-3' (*Eag*);
For:5'-CTACACGCTGGAGCAGCAGaACGGtAccGACCGCTACCTCATCTATGTGG-3' (*Kpn*);
Rev:5'-CCACATAGATGAGGTAGCGGTCggTaCCGTtCTGCTGCTCCAGCGTGTAG-3' (*Kpn*);
For:5'CACGCTGGAGCAGCAGGcCGGGgcGGcCCGgTACCTCATCTATGTGGATGAGAGCC-3' (*Kpn*);
Rev:5'-GGCTCTCATCCACATAGATGAGGTAcCGGgCCgcCCCGgCCTGCTGCTCCAGCGTG-3' (*Kpn*);

PCR amplified DNA was transferred back into the original CD18-containing expression vector using Eco47III and AvrII restriction sites. Each mutation was confirmed by the presence of the introduced restriction site and by DNA sequencing.

Cell Culture and Transfection. Transient transfection assays were carried out in HEK293 cells (American Type Culture Collection) as described [9]. Briefly, HEK293 cells were plated on tissue culture treated p-10 plates (Clontech) and maintained in complete medium consisting of Dulbecco's Modified Eagle Medium (DMEM, Gibco BRL) supplemented with 10% heat-inactivated fetal bovine serum (Gibco BRL) and 50 IU/ml penicillin and streptomycin (Gibco BRL) at 37˚C. The cells were detached with 0.05% Trypsin-EDTA solution (Gibco BRL) and plated in wells of six-well plates at a concentration of 1 million cells per

well. Cells at ~70% confluence were transfected with supercoiled cDNA encoding wild-type (WT) and mutant CD18 together with WT CD11b using Lipofectamine2000 reagent (Invitrogen) and following the manufacturer's protocol. Transfected cells were grown for 24 h at 37˚C in 5% CO_2. Cells were then carefully washed and detached with the 0.05% Trypsin-EDTA solution, counted and seeded in replicates for 24 hours onto poly-L-lysine (SIGMA) coated 48-well plates (Clontech). Confluent monolayers in the 48-wells were then used for integrin cell-surface expression and ligand-binding assays.

Stable transfection of WT and mutant integrins was carried out in K562 cells (from ATCC) using published electroporation protocols [20]. Briefly, K562 cells were grown to log phase in Iscove's Modified Dulbecco's Medium (IMDM, CellGro) supplemented with 10% heat-inactivated fetal bovine serum and 50 IU/ml penicillin and streptomycin, at 37˚C and resuspended in serum-free IMDM at ~1 X 10^7/ml. A total of 0.5 ml of cells were transferred into a 0.4-cm cuvette (Fisher), and 10μg of CD11b WT- and 10μg of WT or mutant CD18 cDNA were added. Electroporation was carried out at 960 μF and 320VC (Gene-Pulser, Bio-Rad Labs). Transfectants were allowed to recover in serum-containing media for 48 h and were then selected with 1mg/ml G418 (GIBCO BRL) for up to two weeks. CD11b/CD18 expressing cells were enriched by FACS Sorting (on BD FACS Sort) using the heterodimer-specific mAb IB4 [20,26]. Sorted cells were cloned by limiting dilution and clones with similar levels of integrin expression were identified by flow cytometry for further analyses. WT and mutant K562 were maintained in IMDM supplemented with 10% heat-inactivated fetal bovine serum, 50 IU/ml penicillin and streptomycin and 1mg/ml G418. K562 cells stably-transfected with WT CD11b/CD18 using the expression plasmid EE6 hCMV carrying a G418-resistance marker were also provided by Dr. D. Simon [27], with similar results.

Preparation of Complement iC3b-coated Sheep Erythrocytes (EiC3b). Sheep erythrocytes (E) coated with complement iC3b were prepared using human serum following published protocols [28]. A slight modification was made in that Hank's Balanced Buffer Solution (HBSS, Gibco BRL) was used instead of the VBSG buffer. Coated and biotinylated erythrocytes (EiC3b and E) were diluted to a concentration of 1.5-6x10^7 cells/ml for the ligand-binding assay.

Antibody and Ligand Binding to HEK293 Cells. Binding of mAbs and EiC3b to transiently transfected HEK293 cells was performed in parallel in 48-well plates as described [9]. Integrin cell surface expression was analyzed using anti-CD11b and anti-CD18 mAbs. Briefly, triplicate wells containing confluent

monolayers of transfected cells, approximately 48 hours post-transfection, were incubated with primary mAbs (10μg/ml) in DMEM buffer containing 0.1% gelatin and 0.02% sodium azide for 1 hour at 4˚C. Binding assays with mAb KIM127 were performed for 30min at 37˚C as described [22,29]. Cells were washed and incubated with biotin-labeled rabbit anti-mouse antibody (Vectastain ABC-kit, Vector Laboratories, CA) for 1 hour at 4˚C, washed three times and subsequently fixed with 1% glutaraldehyde overnight at 4˚C. After blocking, wells were developed using streptavidin-alkaline phosphatase (AP, Vectastain ABC-kit, Vector Laboratories) and p-nitrophenyl phosphate (PNPP, Sigma Chemical Co., MO USA) to generate a colored product. The enzymatic reaction was quenched with equal volumes of 2N NaOH, and 100 μl of this solution was transferred to 96-well plates (Costar) and OD^{405} was measured. Binding results, reported as histograms representing mean$\pm$SD of triplicate wells, were normalized such that binding of each antibody to the WT receptor was considered 100.

Ligand binding was assessed by adding 150μl of EiC3b (60 X 10^6/ml) to triplicate confluent wells in a total volume of 300μl followed by a 15s spin at 500 rpm. After 35 min incubation at 37˚C, wells were washed and subsequently fixed with 1% glutaraldehyde. Wells were developed using AP and PNPP as above and binding quantitated. Specific binding was obtained by subtracting background binding of mock-transfected cells and expressed as percentage of binding to WT obtained in the presence of Ca^{2+}+Mg^{2+} after correcting for expression using mAb IB4 as previously described [30].

Immunoprecipitations. Immunoprecipitation followed by a western blot analysis was carried out to confirm heterodimerization of WT and mutant CD11b/CD18 integrins on the surface of transfected cells. Confluent, transfected HEK 293 cells in six-well plates were extracted using RIPA buffer (Boston Bioproducts) supplemented with 1mg/ml DNase and a cocktail of protease inhibitors (Complete™; Roche Diagnostics). The detergent-soluble fraction was harvested upon centrifugation and immunoprecipitated using the anti-CD11b mAb 44a and Protein G Sepharose-4 (Amersham Pharmacia Biotech AB, Uppsala Sweden). Washed immunoprecipitates were separated by SDS-PAGE on a 4-15% gradient Tris-HCl gel (Bio-Rad Laboratories, CA USA) under reducing conditions and electroblotted onto PVDF membranes (Bio-Rad Laboratories). After blocking with 10% nonfat milk in 25mM Tris-HCl, pH 7.4, 137mM NaCl, 2.7mM KCl (TBS, Boston Bioproducts, MA), the membrane was incubated with a polyclonal anti-CD18 antibody as described [9]. Detection of proteins was performed using horseradish peroxidase (HRP) linked anti-rabbit antibody (Amersham Pharmacia Biotech AB) and SuperSignal® Chemiluminescent kit (Pierce

Chemical Company). The luminescent signal was detected using BioMax x-ray films (Eastman Kodak Company, NY USA).

Flow Cytometry of K562. Flow cytometric analysis of K562 cells was performed using published protocols [31,32]. Briefly, cells were counted and washed twice with TBS. Cells (5 X 10^5) were incubated with primary mAb (10μg/ml) in 100μl TBS on ice for 30 min, except for mAbs 24 and KIM127 and the isotype-matched control mAb MOPC-21, where incubations were performed at 37°C and in the presence of 1mM each of Ca^{2+} and Mg^{2+} or 1mM Mn^{2+} [31]. Cells were then washed with TBS and incubated with FITC-conjugated secondary mAbs on ice for 30 min. Stained cells were washed and resuspended in cold TBS and analyzed using FACS Scan flow cytometer (BD Biosciences, San Jose, CA), counting 10,000 events. Data was analyzed using the CellQuest software (BD Biosciences).

K562 binding to iC3b in suspension. K562 cells were washed twice in TBS, resuspended to 1x10^6/ml of which 40 μl (4x10^4 cells) were incubated in suspension with EiC3b (0.75 X 10^6) in a total volume of 100μl at 37°C for 25 min in the presence of 1mM each of Ca^{2+}+Mg^{2+}, 1mM Mn^{2+}, varying concentrations of Ca^{2+}, or in 5mM EDTA. In preliminary studies, we found that the ~20:1 EiC3b: K562 ratio falls on the steep portion of the dose-response curve and is thus sensitive to changes in ligand-binding activity of the integrin (not shown). Binding, detected in the form of "rosettes" (≥3 EiC3b/K562, >200 cells examined in multiple fields), was scored using phase-contrast microscopy. Binding results are reported as histograms representing mean±SD of triplicate experiments.

K562 binding to iC3b immobilized on microtiter plates. 384-well Maxisorp microtiter plates were coated with 5μg/ml of monomeric iC3b ligand [25] in PBS containing 1mM Ca^{2+} and 1mM Mg^{2+} (PBS^{++}) overnight at 4°C. The concentration of iC3b used for these experiments fell on the steep portion of the dose-response curve (not shown). After coating with iC3b, the wells were washed with TBS and non-specific sites were blocked by incubation with 2% non-fat milk in TBS at room temperature for 30min. The wells were washed three times with TBS and the plates were immediately used in adhesion assays. K562 cells (30,000) were transferred to each well and incubated at room temperature for 30 min in the presence of 1mM each of Ca^{2+}+Mg^{2+}, 1mM Mn^{2+} or 5mM EDTA in a total volume of 100μL. Following a washing step, the adherent cells were fixed with formaldehyde (1.1%v/v final concentration), washed three more times with TBS and the adherent cells were fluorescently labeled with DAPI (0.5μM final in TBS with

0.1% TritonX-100) and quantitated using automated microscope (CellWorx automated microscope, Cellomics, PA) set at 0.3s exposure using DAPI filter set to capture 1-3 images per well. Digitized photomicrographs were then analyzed using MetaXpress image analysis software (Molecular Devices, CA) using the built-in cell count module to quantify nuclear staining. Data output files were analyzed using MS Excel.

Cell spreading Assay. 384-well Maxisorp microtiter plates coated with 5μg/ml iC3b ligand were prepared as described above. K562 cells (20,000) were transferred to each well and incubated at room temperature for 1.5 hours in serum-free IMDM, then processed as above and cell spreading visualized (>200 cells examined in multiple fields) using phase-contrast microscopy. Spreading results are reported as histograms representing mean $\pm$ SD of triplicate determinations from three separate experiments.

Results

Expression of mutant forms of CD11b/CD18 in HEK293 cells. We modified the βTD's CD loop residues D658GMD of WT CD18 (Figure 1, inset) by swapping them with the equivalent D672SSG residues of the β3-subunit. The D658GMD sequence was also replaced with AGAA or with NGTD (to fashion a neo N-glycan at N658). We assessed transient expression of mutant CD11b/CD18 integrins on the surface of HEK293 cells, which lack endogenous CD11b/CD18, using the heterodimer-specific mAb IB4 and the CD11b-specific mAb 44a. Figure 2A shows that all three CD loop mutants were expressed on the surface of HEK293 cells but at reduced levels (~50% of that of the WT integrin). Both the 44a and IB4 mAbs registered a similar level of integrin expression, which suggests that the expressed integrins are in their heterodimeric form. We further verified integrin heterodimer formation by immunoprecipitation from detergent HEK293 cell lysates with mAb 44a followed by western blotting using polyclonal anti-CD18 antibody (Figure 2B). Autoradiograph of the western blot shows the presence of comparable amounts of CD18 in immunoprecipitates from HEK293 cells expressing WT or mutant integrins (Lanes 1-4), suggesting that equivalent amounts are being synthesized. The slower mobility of the NGTD CD18 mutant (lane 4) is consistent with the attachment of a neo N-glycan at the introduced site [13]. No CD18 was seen in anti-CD11b immunoprecipitates from mock-transfected HEK293 cells (lane 5).

The βTD-modified CD11b/CD18 integrins are active in HEK293. Binding of CD11b/CD18 to its physiologic ligands including iC3b is divalent-cation and activation-dependent [30,33]. We therefore used the

iC3b ligand to assess the functional impact of modifying the βTD CD loop in the CD11b/CD18 mutants expressed on the surface of HEK293 in the physiologic divalent cations (Ca^{2+} plus Mg^{2+}, each at 1mM). A portion of the WT CD11b/CD18 expressed on HEK293 assumes the active state [34], explaining its intrinsic binding to EiC3b (Figure 2C). Binding of the βTD mutants to EiC3b increased by 2-3 fold above that of the WT receptor (set empirically at 100%) (Figure 2C). This level of binding did not increase further by the activating cation Mn^{2+} (at 1mM) (Figure 2C), commonly used as a mimic of inside-out integrin activation (reviewed in [1]), suggesting that the majority of the expressed receptors are already activated.

The βTD-modified CD11b/CD18 is constitutively active in K562. The nature of the conformational changes that may occur in parallel with the high affinity (physiologic ligand binding state) were next examined in more detail in the βTD mutants expressed stably in K562 cells. K562 cells express WT integrins in a default low affinity state as in normal leukocytes [35], which can be activated by inside-out signals primarily through a change in integrin affinity rather than avidity [36], thereby providing a more relevant context to observe changes in the level of integrin activation [35]. K562 cells expressing equivalent levels of heterodimeric WT and mutant CD11b/CD18 (Figure 3A) were examined for their ability to bind iC3b (covalently bound to the surface of erythrocytes using fresh serum, as in the physiologic state) or adsorbed to microtiter plastic plates. In the presence of the physiologic divalent cations, binding (rosette formation) of the mutant CD11b/CD18 receptors to EiC3b in suspension was constitutive, unlike that of the WT, which was minimal (≤20%). Mn^{2+} increased the level of binding of the WT to the same degree seen in the mutants in physiologic cations, but did not induce a further increase in EiC3b binding by the mutants (Figure 3B), indicating that the respective integrin mutants are maximally activated in this assay, as in HEK293. We also performed a titration with increasing numbers of EiC3b to a constant concentration of WT, NGTD or mock K562 cells. Results, presented in Figure 3C, show that even at very low numbers of EiC3b (and thus, a low EiC3b/K562 cell ratio), the mutant NGTD-expressing K562 cells showed higher binding to EiC3b in physiologic cations compared to WT-expressing cells. These differences were most pronounced at an EiC3b/K562 cell ratio of ~18. While Mn^{2+} produced the expected increase in binding of WT-expressing K562 to EiC3b, no increase in EiC3b binding to the NGTD mutant took place at any EiC3b/K562 cell ratio tested.

We also evaluated ligand binding under conditions in which CD11b/CD18-expressing K562 were allowed to bind ligand adsorbed onto microtiter plastic plates. The specificity of the interaction was again reflected

in the lack of binding of mock K562 or WT CD11b/CD18 expressing K562 in the presence of the physiologic divalent cations (Figure 4A), while 1mM Mn^{2+} was sufficient to induce maximal binding by the WT receptor. K562 expressing the βTD mutant CD11b/CD18 receptors all showed significant binding to immobilized iC3b in the presence of physiologic cations. However and in contrast to the rosetting assay and the binding assay in HEK293, there were small but significant differences in the magnitude of the response to the addition of Mn^{2+}; in the case of the NGTD mutant, Mn^{2+} produced only a modest increase in iC3b binding above that seen in Ca^{2+}+Mg^{2+}, but the increase was more in the case of the DSSG and even higher in the case of the AGAA mutant (Figure 4A).

The CD11b/CD18 βTD mutants show increased cell spreading. To determine whether the activating βTD mutations also modify outside-in signaling, we measured cell spreading on iC3b-coated plates in the presence of Ca^{2+}+Mg^{2+} (1mM each). Both mock and WT CD11b/CD18-expressing K562 cells showed minimal cell spreading (Figures 4B-C). All three βTD mutants showed increased cell spreading, with the NGTD mutant presenting the maximal level of spreading, followed by DSSG and AGAA.

Reactivity of βTD-modified CD11b/CD18 with conformationally sensitive mAbs. We next used mAbs to probe the conformational state of the expressed mutants in K562. mAb 24 is widely used as a reporter of the high affinity state in β2 integrins [23]. It binds to an activation- and cation- dependent epitope in βA, which includes residues Arg122 of the α1' helix and Glu175 in the specificity determining loop (SDL) [31] (Figure 1). We assessed the binding of this mAb to WT- and mutant CD11b/CD18 expressed on K562. AGAA, DSSG and NGTD mutants showed a significant increase in binding to mAb24 compared to WT (Figure 5). The magnitude of this increase was similar to that observed in maximally activated β2 integrins expressed in K562 [37] or in Jurkat cells [38]. In the presence of Mn^{2+}, the reactivity of mAb 24 with WT increased by ~3-fold, compared to the 1.5-1.8 fold increase seen in the case of the mutant integrins (Figure 5).

mAb KIM127 binds an epitope in the EGF2 domain in genu-straightened β2-inetgrins [39], and has therefore been used as a marker of this state [40]. Since WT CD11b/CD18 is largely inactive when expressed on K562, whereas all three mutants are constitutively active as judged by the iC3b binding assays, we tested mAb KIM127 binding to WT and βTD mutant receptors in physiologic Ca^{2+}+Mg^{2+}. There was no significant

difference in the level of binding of mAb KIM127 to the constitutively active βTD mutants vs. the WT receptor (Figure 6). Reactivity of mAb KIM127 to the WT integrin was doubled in the presence of 1mM Mn^{2+}, a level of increase consistent with previous reports [38]. Interestingly, Mn^{2+} produced an equivalent increase in binding of mAb KIM127 to each of the three βTD mutants (Figure 6).

Discussion

Previous studies in the ligand-binding integrin αA domain have shown that the transition from the inactive to the active state involves coordinated changes in the α1 helix, the F/α7 loop and α7 helix (reviewed in [41]). Small molecules or certain mAbs that bind in the F/α7 region allosterically block ligand binding [42,43]. The membrane-proximal βTD in the bent integrin contacts βA in the F-α7 region; replacing the contact residues S674 (from the βTD CD loop) and V332 (from the βA F-strand) with cysteines creates a disulphide bridge that locks the membrane-bound integrin in the low affinity state [11,44]. Here we show that modifications of the CD loop in the β2 integrin CD11b/CD18 are activating, suggesting that the βTD acts as an allosteric regulator of ligand binding in this integrin. Constitutive activation of the integrin by the CD loop mutations also led to a proportional increase in cell spreading on iC3b-coated surfaces, an outside-in signaling response.

The crystal structure of the bent integrin shows that the βA F/α7 loop is also stabilized in the low affinity state, through an ADMIDAS metal ion-mediated bridge to the α1 helix, which prevents the inward movement of this helix and the restructuring of the F/α7 loop during activation (Figure 1, inset)(reviewed in [41]). This link is unique to βA domains (vs. the αA domains) and is broken in the crystal structure of the RGD-bound bent integrin ectodomain [3]. Mutational removal of this link also generates constitutively active bent β2 integrins, but impairs cell spreading (data not shown and [45]), the latter effect perhaps reflective of the need for the ADMIDAS ion in stabilizing the liganded (signaling) integrin state as well [41]. Other studies have shown that swapping of the βA's F/α7 loop residues in β2 with those in the β1-subunit or replacing certain residues with alanine induced the high affinity state in the respective integrin [46,47]. Taken together, these data argue that local conformational changes taking place within βA or its contact with the βTD are sufficient to switch the integrin to high binding affinity.

Binding of K562-expressing βTD mutants to EiC3b in suspension was equivalent in the presence of physiologic Ca^{2+} +Mg^{2+} or Mn^{2+}, over a broad range of ligand concentrations (Figure 3B, C). This was also the case when EiC3b was allowed to bind to adherent HEK293 cells (Figure 2C). However, only in the case of the NGTD-expressing K562 did binding to the adsorbed iC3b in Ca^{2+}+Mg^{2+} approach that seen in the presence of the activating Mn^{2+}. Mn^{2+} produced a significant increase in binding of AGAA- and to a lesser degree DSSG-expressing K562 to iC3b above that obtained in Ca^{2+}+Mg^{2+} (Figure 4A). Also, Mn^{2+} further increased the constitutive binding of the affinity reporter mAb24 to all three βTD mutants (Figure 5). One interpretation of these findings is that the βTD mutations increase both receptor avidity as well as affinity. It is known however that the change in physiologic ligand binding to integrins expressed in K562 reflects an affinity rather than an avidity switch [36]. If a change in avidity is also operational, it is more likely to impact integrin binding to the plastic adsorbed purified ligand. A second interpretation is that the AGAA and DSSG mutants may exert a priming effect, enhancing the transition from the low- to the high-affinity state, short of the full activation state induced by Mn^{2+}. This priming effect is more likely detected when receptor-carrying cells are in suspension, as in the adsorbed ligand-binding assay, explaining the selective enhancing effect of Mn^{2+} in this case. The nearly equivalent ligand binding activity of the NGTD mutant in Ca^{2+}+Mg^{2+} or Mn^{2+} in all three ligand-binding assays performed indicate however that this mutation is most effective in inducing the activation state. Why then is its binding to mAb24 incomplete unless Mn^{2+} is present? It is likely that the incremental increase in mAb24 binding to NGTD-expressing K562 by Mn^{2+} reflects the small but significant enhancement observed in ligand binding by this cation (Figure 4A). It is also known that mAb24 reports ligand-occupied βA [48]- in αA-containing integrins, the endogenous high affinity αA domain engages the βA MIDAS through the MIDAS cation, which allows αA to then bind exogenous physiologic ligands like iC3b (the ligand relay model) [9]. Thus, the Mn^{2+}-induced further increase in binding of mAb24 (vs. iC3b ligand) to the NGTD mutant may reflect the preferential coordination of αA-occupied βA by Mn^{2+} at MIDAS, in comparison to Mg^{2+} or Ca^{2+}.

It could be argued that more complete activation of CD11b/CD18 by the NGTD mutation may be the result of the bulky sugar moiety breaking the additional contacts the βTD makes with the hybrid domain [2] (Figure 1), resulting in head-leg separation, genu-straightening and the opening of the βA/hybrid hinge, all believed to be features of the high affinity state [13,39]. However, mAb KIM127, used as the reporter of the genu-straightened conformation of the integrin [31] did not bind to the βTD mutants, in particular NGTD, in the

presence of Ca^{2+}+Mg^{2+} (Figure 6). Mn^{2+} exposed the KIM127 eiptope in both WT and the βTD mutants to the same degree. This finding together with the physiologic ligand binding data suggests that integrin activation can take place in the absence of genu-straightening, which has been linked to the opening of the βA/hybrid hinge. Consistently, the high binding affinity ADMIDAS-defective CD11a/CD18 integrin was also found to be poorly reactive with KIM127 [45], and fluorescence lifetime imaging (FLIM) analysis in intact K562 cells in the presence of physiologic cations shows that the ligand-binding site in WT and the NGTD mutant CD11b/CD18 is unchanged relative to the lipid bilayer, arguing against genu-straightening induced by this mutation (manuscript in preparation). Finally, a recent molecular dynamics study [49] found that the activating inward shift of the βA α1 helix can be achieved with a very modest ~20^o opening of the βA/hybrid hinge; an increase of this magnitude can be accommodated in the ligand-bound bent conformation [14].

The results presented here add new insights into the allosteric pathways resulting in the integrin-activated state (Figure 7). In the low-affinity state, the integrin is likely expressed on the cell surface in a bent conformation (Figure 7A), stabilized by head to leg contacts, inclusive of the membrane-proximal βTD. Conformational changes in the cytoplasmic tails and transmembrane helices, generated by inside-out activation, likely produce a βTD/βA hinge opening (Figure 7B), which switches the integrin βA to the high affinity binding state, manifested by the restructuring of the F/α7 loop, disrupting ADMIDAS which permits the activating inward movement of the α1 helix needed to create as stable ligand-binding MIDAS. We cannot exclude a modest (≤ 20^o) [14] opening of the βA/hybrid hinge in the bent integrin as part of this process. The strain build-up induced by the binding of physiologic ligand to the bent high affinity integrin is released by various degrees of opening of the βA/hybrid hinge (Figure 7C, D), that likely extend to those seen in the crystal structure of the ligand-bound αIIbβ3 head segment [5], eliciting genuextension and leg separation, which likely characterize the outside-in signaling state.

In conclusion, we have shown that the βTD CD loop in the bent CD11b/CD18 integrin is functionally relevant, playing an important role in inside-out integrin activation, as proposed in the deadbolt model [32]. Additional accumulating evidence may now be explained in this light (reviewed in [41,50]). For example, creating a disulphide linkage between the βTD and calf-2 has been shown to block activation [44]; this may prevent the βTD/βA hinge movement. Similarly, mutation of each of the four cysteine pairs present in the

βTD domain revealed that only C663-C687 in the β3-subunit, located at the base of the CD loop five residues away from the TM segment (Figure 1), is activating when interrupted [50]. Of interest in this regard is that the βTD's CD loop and the strands, inclusive of the stabilizing disulphide at its base, are naturally absent in the β8-subunit in vertebrates [51]; the present data suggest that these modifications may prime or activate the respective β8 integrin.

Acknowledgments

We thank Dr. Martyn Robinson for providing mAb KIM127, Dr. Nancy Hogg for providing mAb 24, and Dr. Jun Park for help with the plate adhesion assays. This research was supported by grants DK48549, DK50305 and DK068253 from the National Institutes of Health.

References

1. Hynes RO. Integrins: bidirectional, allosteric signaling machines. Cell. 2002;110:673-687.
2. Xiong JP, Stehle T, Diefenbach B, et al. Crystal structure of the extracellular segment of integrin alpha Vbeta3. Science. 2001;294:339-345.
3. Xiong JP, Stehle T, Zhang R, et al. Crystal structure of the extracellular segment of integrin alpha Vbeta3 in complex with an Arg-Gly-Asp ligand. Science. 2002;296:151-155.
4. Xiong JP, Stehle T, Goodman SL, Arnaout MA. A novel adaptation of the integrin PSI domain revealed from its crystal structure. J Biol Chem. 2004;279:40252-40254.
5. Xiao T, Takagi J, Coller BS, Wang JH, Springer TA. Structural basis for allostery in integrins and binding to fibrinogen-mimetic therapeutics. Nature. 2004;432:59-67.
6. Lee JO, Rieu P, Arnaout MA, Liddington R. Crystal structure of the A domain from the alpha subunit of integrin CR3 (CD11b/CD18). Cell. 1995;80:631-638.
7. Lee JO, Bankston LA, Arnaout MA, Liddington RC. Two conformations of the integrin A-domain (I-domain): a pathway for activation? Structure. 1995;3:1333-1340.
8. Emsley J, Knight CG, Farndale RW, Barnes MJ, Liddington RC. Structural basis of collagen recognition by integrin alpha2beta1. Cell. 2000;101:47-56.
9. Alonso JL, Essafi M, Xiong JP, Stehle T, Arnaout MA. Does the integrin alphaA domain act as a ligand for its betaA domain? Curr Biol. 2002;12:R340-342.
10. Nermut MV, Green NM, Eason P, Yamada SS, Yamada KM. Electron microscopy and structural model of human fibronectin receptor. EMBO J. 1988;7:4093-4099.
11. Takagi J, Petre BM, Walz T, Springer TA. Global conformational rearrangements in integrin extracellular domains in outside-in and inside-out signaling. Cell. 2002;110:599-511.
12. Calzada MJ, Alvarez MV, Gonzalez-Rodriguez J. Agonist-specific structural rearrangements of integrin alpha IIbbeta 3. Confirmation of the bent conformation in platelets at rest and after activation. J Biol Chem. 2002;277:39899-39908.
13. Luo BH, Springer TA, Takagi J. Stabilizing the open conformation of the integrin headpiece with a glycan wedge increases affinity for ligand. Proc Natl Acad Sci U S A. 2003;100:2403-2408.
14. Adair BD, Xiong JP, Maddock C, Goodman SL, Arnaout MA, Yeager M. Three-dimensional EM structure of the ectodomain of integrin {alpha}V{beta}3 in a complex with fibronectin. J Cell Biol. 2005;168:1109-1118.

15. Salas A, Shimaoka M, Phan U, Kim M, Springer TA. Transition from rolling to firm adhesion can be mimicked by extension of integrin alphaLbeta2 in an intermediate affinity state. J Biol Chem. 2006;281:10876-10882.

16. Ginsberg MH, Partridge A, Shattil SJ. Integrin regulation. Curr Opin Cell Biol. 2005;17:509-516.

17. Arnaout MA, Todd RF, 3rd, Dana N, Melamed J, Schlossman SF, Colten HR. Inhibition of phagocytosis of complement C3- or immunoglobulin G-coated particles and of C3bi binding by monoclonal antibodies to a monocyte-granulocyte membrane glycoprotein (Mol). J Clin Invest. 1983;72:171-179.

18. Sanchez-Madrid F, Simon P, Thompson S, Springer TA. Mapping of antigenic and functional epitopes on the alpha- and beta-subunits of two related mouse glycoproteins involved in cell interactions, LFA-1 and Mac-1. J Exp Med. 1983;158:586-602.

19. Wright SD, Rao PE, Van Voorhis WC, et al. Identification of the C3bi receptor of human monocytes and macrophages by using monoclonal antibodies. Proc Natl Acad Sci U S A. 1983;80:5699-5703.

20. Hogg N, Stewart MP, Scarth SL, et al. A novel leukocyte adhesion deficiency caused by expressed but nonfunctional beta2 integrins Mac-1 and LFA-1. J Clin Invest. 1999;103:97-106.

21. Dana N, Clayton LK, Tennen DG, et al. Leukocytes from four patients with complete or partial Leu-CAM deficiency contain the common beta-subunit precursor and beta-subunit messenger RNA. J Clin Invest. 1987;79:1010-1015.

22. Robinson MK, Andrew D, Rosen H, et al. Antibody against the Leu-CAM beta-chain (CD18) promotes both LFA-1- and CR3-dependent adhesion events. J Immunol. 1992;148:1080-1085.

23. Dransfield I, Hogg N. Regulated expression of Mg2+ binding epitope on leukocyte integrin alpha subunits. EMBO J. 1989;8:3759-3765.

24. Sambrook J, Fritsch EF, Maniatis T. Molecular Cloning: A Laboratory Manual, Second Edition (Cold Spring Harbor Laboratory, Cold Spring Harbor, NY). 1989.

25. Li R, Arnaout MA. Functional analysis of the beta 2 integrins. Methods Mol Biol. 1999;129:105-124.

26. Tan SM, Hyland RH, Al-Shamkhani A, Douglass WA, Shaw JM, Law SK. Effect of integrin beta 2 subunit truncations on LFA-1 (CD11a/CD18) and Mac-1 (CD11b/CD18) assembly, surface expression, and function. J Immunol. 2000;165:2574-2581.

27. Simon DI, Xu H, Ortlepp S, Rogers C, Rao NK. 7E3 monoclonal antibody directed against the platelet glycoprotein IIb/IIIa cross-reacts with the leukocyte integrin Mac-1 and blocks adhesion to fibrinogen and ICAM-1. Arterioscler Thromb Vasc Biol. 1997;17:528-535.

28. Michishita M, Videm V, Arnaout MA. A novel divalent cation-binding site in the A domain of the beta 2 integrin CR3 (CD11b/CD18) is essential for ligand binding. Cell. 1993;72:857-867.

29. Dransfield I, Cabanas C, Craig A, Hogg N. Divalent cation regulation of the function of the leukocyte integrin LFA-1. J Cell Biol. 1992;116:219-226.

30. Li R, Rieu P, Griffith DL, Scott D, Arnaout MA. Two functional states of the CD11b A-domain: correlations with key features of two Mn2+-complexed crystal structures. J Cell Biol. 1998;143:1523-1534.

31. Lu C, Ferzly M, Takagi J, Springer TA. Epitope mapping of antibodies to the C-terminal region of the integrin beta 2 subunit reveals regions that become exposed upon receptor activation. J Immunol. 2001;166:5629-5637.

32. Xiong JP, Stehle T, Goodman SL, Arnaout MA. New insights into the structural basis of integrin activation. Blood. 2003;102:1155-1159.

33. Xiong JP, Li R, Essafi M, Stehle T, Arnaout MA. An isoleucine-based allosteric switch controls affinity and shape shifting in integrin CD11b A-domain. J Biol Chem. 2000;275:38762-38767.

34. Shimaoka M, Shifman JM, Jing H, Takagi J, Mayo SL, Springer TA. Computational design of an integrin I domain stabilized in the open high affinity conformation. Nat Struct Biol. 2000;7:674-678.

35. Ortlepp S, Stephens PE, Hogg N, Figdor CG, Robinson MK. Antibodies that activate beta 2 integrins can generate different ligand binding states. Eur J Immunol. 1995;25:637-643.

36. Beals CR, Edwards AC, Gottschalk RJ, Kuijpers TW, Staunton DE. CD18 activation epitopes induced by leukocyte activation. J Immunol. 2001;167:6113-6122.

37. Annenkov A, Ortlepp S, Hogg N. The beta 2 integrin Mac-1 but not p150,95 associates with Fc gamma RIIA. Eur J Immunol. 1996;26:207-212.

38. Cherry LK, Li X, Schwab P, Lim B, Klickstein LB. RhoH is required to maintain the integrin LFA-1 in a nonadhesive state on lymphocytes. Nat Immunol. 2004;5:961-967.

39. Nishida N, Xie C, Shimaoka M, Cheng Y, Walz T, Springer TA. Activation of Leukocyte beta(2) Integrins by Conversion from Bent to Extended Conformations. Immunity. 2006;25:583-594.

40. Yang W, Shimaoka M, Salas A, Takagi J, Springer TA. Intersubunit signal transmission in integrins by a receptor-like interaction with a pull spring. Proc Natl Acad Sci U S A. 2004;101:2906-2911.

41. Arnaout MA, Mahalingam B, Xiong JP. Integrin Structure, Allostery, And Bidirectional Signaling. Annu Rev Cell Dev Biol. 2005;21:381-410.

42. Kallen J, Welzenbach K, Ramage P, et al. Structural basis for LFA-1 inhibition upon lovastatin binding to the CD11a I-domain. J Mol Biol. 1999;292:1-9.

43. Li R, Haruta I, Rieu P, Sugimori T, Xiong JP, Arnaout MA. Characterization of a conformationally sensitive murine monoclonal antibody directed to the metal ion-dependent adhesion site face of integrin CD11b. J Immunol. 2002;168:1219-1225.

44. Kamata T, Handa M, Sato Y, Ikeda Y, Aiso S. Membrane-proximal {alpha}/{beta} stalk interactions differentially regulate integrin activation. J Biol Chem. 2005;280:24775-24783.

45. Chen J, Yang W, Kim M, Carman CV, Springer TA. Regulation of outside-in signaling and affinity by the beta2 I domain of integrin alphaLbeta2. Proc Natl Acad Sci U S A. 2006;103:13062-13067.

46. Ehirchiou D, Xiong YM, Li Y, Brew S, Zhang L. Dual function for a unique site within the beta2I domain of integrin alphaMbeta2. J Biol Chem. 2005;280:8324-8331.

47. Hato T, Yamanouchi J, Yakushijin Y, Sakai I, Yasukawa M. Identification of critical residues for regulation of integrin activation in the beta6-alpha7 loop of the integrin beta3 I-like domain. J Thromb Haemost. 2006;4:2278-2280.

48. Shimaoka M, Salas A, Yang W, Weitz-Schmidt G, Springer TA. Small molecule integrin antagonists that bind to the beta2 subunit I-like domain and activate signals in one direction and block them in the other. Immunity. 2003;19:391-402.

49. Puklin-Faucher E, Gao M, Schulten K, Vogel V. How the headpiece hinge angle is opened: new insights into the dynamics of integrin activation. J Cell Biol. 2006;175:349-360.

50. Kamata T, Ambo H, Puzon-McLaughlin W, et al. Critical cysteine residues for regulation of integrin alphaIIbbeta3 are clustered in the epidermal growth factor domains of the beta3 subunit. Biochem J. 2004;378:1079-1082.

51. Jannuzi AL, Bunch TA, West RF, Brower DL. Identification of integrin beta subunit mutations that alter heterodimer function in situ. Mol Biol Cell. 2004;15:3829-3840.

FIGURE LEGENDS

Figure 1. Spatial relationships of the βTD domain. A Ribbon diagram of a model of CD11b/CD18 based on the crystal structure of unliganded αVβ3 ectodomain [2]. The eight β2-subunit domains (in front) are labeled. The five CD11b-subunit domains αA (MIDAS ion in cyan), propeller (with four metal ions, orange spheres), thigh and calf-1 and 2 (light gray) are labeled. The metal ion in the α-genu (arrow) is in orange. The specificity-determining loop (SDL) in βA is indicated by an arrowhead. The C663-C687 disulphide bridge found at the bottom of the CD-loop is shown (colored cyan). The position of the plasma membrane (PM) is indicated by a dotted line for orientation. *Inset*: an enlarged image of the βTD's CD loop (brown, arrow) and F/α7 region (red) in the unliganded αVβ3 ectodomain [2]. The ADMIDAS ion (magenta) links the α1'- α1 helix and F/α7 loop through D126D127 and M335 (equivalent to D119D120, E325 in the β2-subunit, respectively)(Cα is in green and oxygens are in red). S123 in β3 (and S116 in β2) complete the metal coordination sphere.

Figure 2. **Surface expression and iC3b binding of WT and mutant CD11b/CD18 in HEK293 cells.** (**A**) Histograms showing the relative binding of the heterodimer-specific mAb IB4 and the anti-CD11b mAb 44a to HEK293 cells expressing WT and βTD mutant CD11b/CD18 receptors. Binding of the respective antibody to the WT receptor was considered 100. Each histogram represents mean $\pm$ SD of triplicate determinations from a representative experiment (one of three performed). (B) Western blots following 4-15% gradient SDS-PAGE showing the presence of CD18 in anti-CD11b (using mAb 44a) immunoprecipitates from HEK293 cells expressing WT (lane 1), AGAA (lane 2), DSSG (lane 3), NGTD CD11b/CD18 mutants and mock-transfected cells (lane 5). Approximately equivalent amounts of the immunoprecipitated receptors were loaded in each lane. The shift in CD18 in the NGTD mutant (lane 4) is consistent with attachment of a neo N-glycan. Arrowheads indicate molecular weight markers at 100kDa and 75kDa (High MW Markers, Boston Bioproducts). No CD18 was seen in anti-CD11b immunoprecipitates from mock-transfected HEK293 cells (lane 5). (C) Histograms showing the relative binding of EiC3b to WT and βTD mutant CD11b/CD18 in buffer containing EDTA (5mM), Ca^{2+}+Mg^{2+} (1mM each) or Mn^{2+} (1mM) and expressed as percentage of binding to WT obtained in the presence of 1mM each of Ca^{2+}+Mg^{2+} after correcting for expression using mAb IB4 as described [9]. Similar results were obtained when the activation-insensitive mAb 44a was used as reference (not shown). Each histogram

represents mean ± SD of triplicate determinations from a representative experiment (one of three performed).

Figure 3. Physiologic ligand binding of K562 stably expressing WT and βTD mutant CD11b/CD18. (**A**) Cell surface expression of CD11b/CD18 on K562 cells using flow cytometry. K562 cells were immunostained with the primary heterodimer specific mAb IB4 (thick lines, unshaded area) or isotype-matched control mAb MOPC-173 (gray shaded area), washed then developed with FITC-rat anti-mouse IgG2a and analyzed, counting 10,000 events. Median fluorescence intensity for mAb IB4 staining is shown in each panel. (**B**) Histograms showing the relative binding of iC3b to WT and mutant CD11b/CD18 in buffer containing 5mM EDTA, 1mM each of Ca^{2+}+Mg^{2+} or 1mM Mn^{2+} and expressed as the number of cells showing rosettes (>3 EiC3b bound per K562 cell) as a percentage of total number of cells counted in a rosetting assay. Each histogram represents mean ± SD of triplicate determinations from a representative experiment (one of three performed). No binding was observed in EDTA and with mock-transfected cells. Details of the methods used are described in Materials and Methods. (**C**) A titration ligand binding curve showing ligand binding (% rosetting) of an increasing number of EiC3b to a constant number of WT- of NGTS-mutant CD11b/CD18 expressing K562 cells in buffer containing 1mM each of Ca^{2+}+Mg^{2+} or 1mM Mn^{2+} (as labeled). Each data point represents mean ± SD of triplicate determinations. Not shown are rosetting results from mock-transfected cells (zero rosettes under all three buffer conditions). The graph shows that NGTD expressing cells have higher percentage of rosetting in physiologic buffer cells under all conditions tested, as compared to WT cells. The difference is greatest when ligand is limiting (at EiC3b/K562 cell ratio of ~18). No difference is seen in mutant integrin binding to iC3b in the presence of Ca^{2+}+Mg^{2+} or Mn^{2+} at all ratios used.

Figure 4. Binding and spreading by WT and βTD mutant CD11b/CD18 to iC3b-coated plates. (**A**) Histograms showing the relative binding of mock-, WT- and mutant CD11b/CD18 expressing cells to iC3b-coated plates in buffer containing 1mM each of Ca^{2+} and Mg^{2+} or 1mM Mn^{2+} and expressed as the absolute number of adherent cells per well. Each histogram represents mean ± SD of triplicate determinations from a representative experiment (one of two performed). Details of the methods used are described in Materials and Methods. No iC3b binding was seen with mock-, WT- or mutant CD11b/CD18 in the presence of EDTA (not shown). (**B**) Histograms showing the relative level of spreading by mock-, WT- and mutant CD11b/CD18 cells to iC3b-coated plates in buffer containing 1mM each of Ca^{2+} and

Mg^{2+} and expressed as a percent of spread cells in the total field (>200 cells examined in multiple fields using phase-contrast microscopy). Spreading results are reported as histograms representing mean $\pm$ SD of triplicate experiments. Details of the methods used are described in Materials and Methods. (**C**) Phase-contrast microscopy images showing the morphology of the cells (mock, WT- and mutant CD11b/CD18) after adhering to iC3b-coated plates for ~1.5 hours in buffer containing 1mM each of Ca^{2+} and Mg^{2+}.

Figure 5. Reactivity of WT and βTD mutant CD11b/CD18 with conformation-sensitive mAb 24. FACS analysis of the reactivity of mAb 24 with WT and mutant CD11b/CD18-expressing K562 cells. Level of CD11b/CD18 surface expression was analyzed using mAb IB4. Mean fluorescence intensity (MFI) values for mAb staining are shown in each panel from a representative experiment (one of three performed), except that MFI of mAb 24 staining is shown after subtraction of the background mock fluorescence staining levels and after normalization to the IB4 expression values.

Figure 6. Reactivity of WT and βTD mutant CD11b/CD18 with genu-extension dependent mAb KIM127. FACS analysis of the reactivity of mAb KIM127 with WT and mutant CD11b/CD18 expressing K562 cells. Level of CD11b/CD18 surface expression was analyzed using mAb IB4. MFI values for mAb staining are shown in each panel from a representative experiment (one of three performed), except that mean fluorescence intensity of KIM127 staining is shown after subtraction of the background mock fluorescence staining levels and after normalization to the IB4 expression values. No binding was observed with isotype control mAb (not shown).

Figure 7. A mechanistic model for the conformational changes during integrin activation and signaling. (**A**) Schematic of the domain structure of low affinity leg-bent CD11b/CD18 (CD11b and CD18 in dark and light gray, respectively). βTD contacts the βA and Hybrid domains and the two legs are in close proximity. The αA is occupied by a metal ion in the low affinity MIDAS (marked with asterisk); the bottom of α7 helix of inactive αA (shown with a thick black arrow) is not engaged by βA. (**B**) Inside-out activation disrupts the βTD contact with βA, which unlocks the βA F/α7 loop and allows the inward shift of the α1 helix leading to the formation of a stable αA-bound βA MIDAS (marked with asterisk) which in turn stabilizes αA in the open (high affinity state) (open semicircle). (**C, D**) Ligand (L) (black circle on a stick) bound at αA MIDAS stabilizes the occupancy of βA MIDAS by endogenous αA, opening up the

βA/hybrid hinge to different degrees (double headed arrows), with larger hinge opening forcing genuextension and leg separation (**D**), resulting in outside-in signaling. See text for additional details.

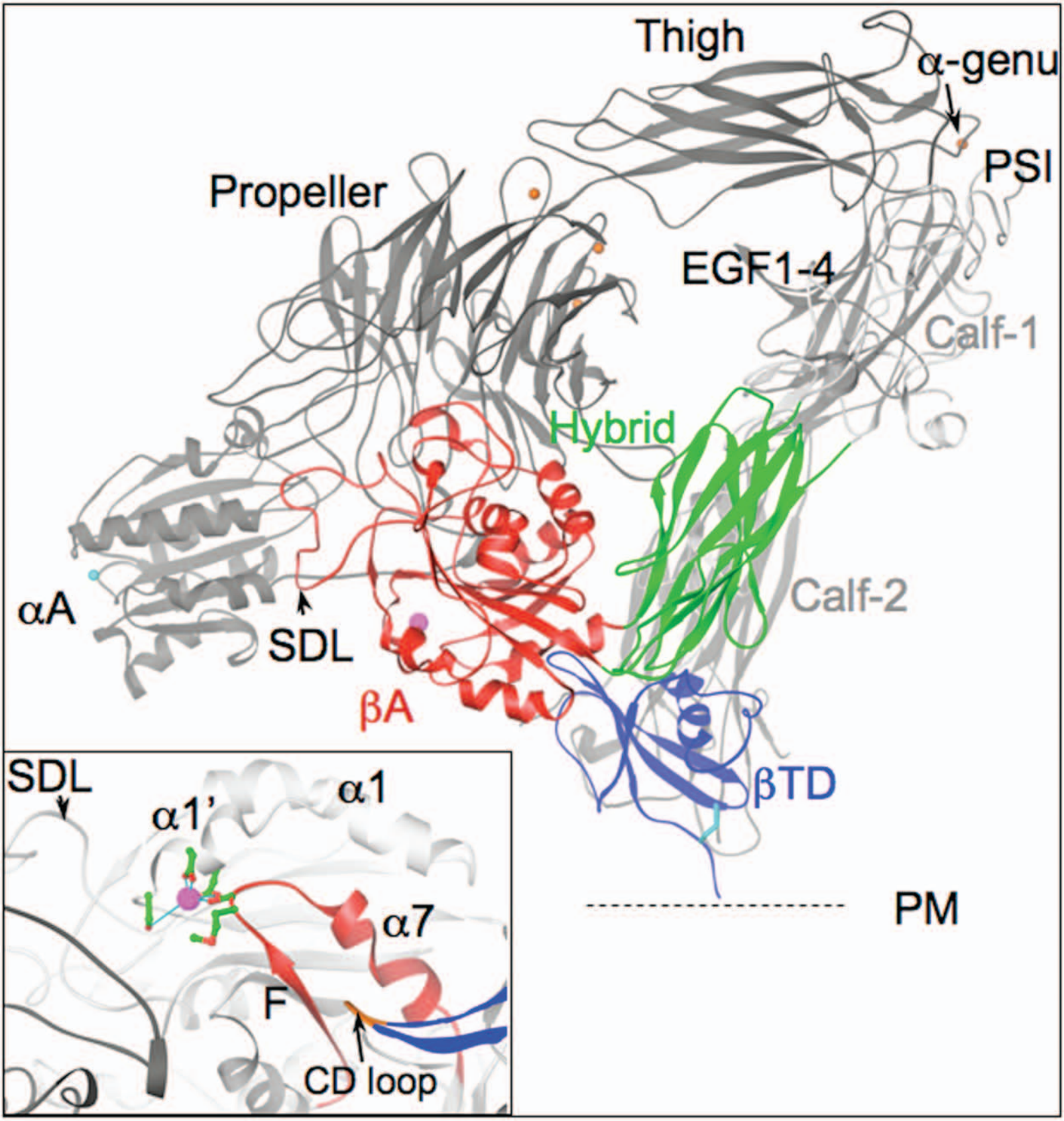
Thigh
α-genu
PSI
Propeller
EGF1-4
Calf-1
Hybrid
αA
SDL
Calf-2
βA
βTD
PM
SDL
α1'
α1
α7
F
CD loop

Figure 1

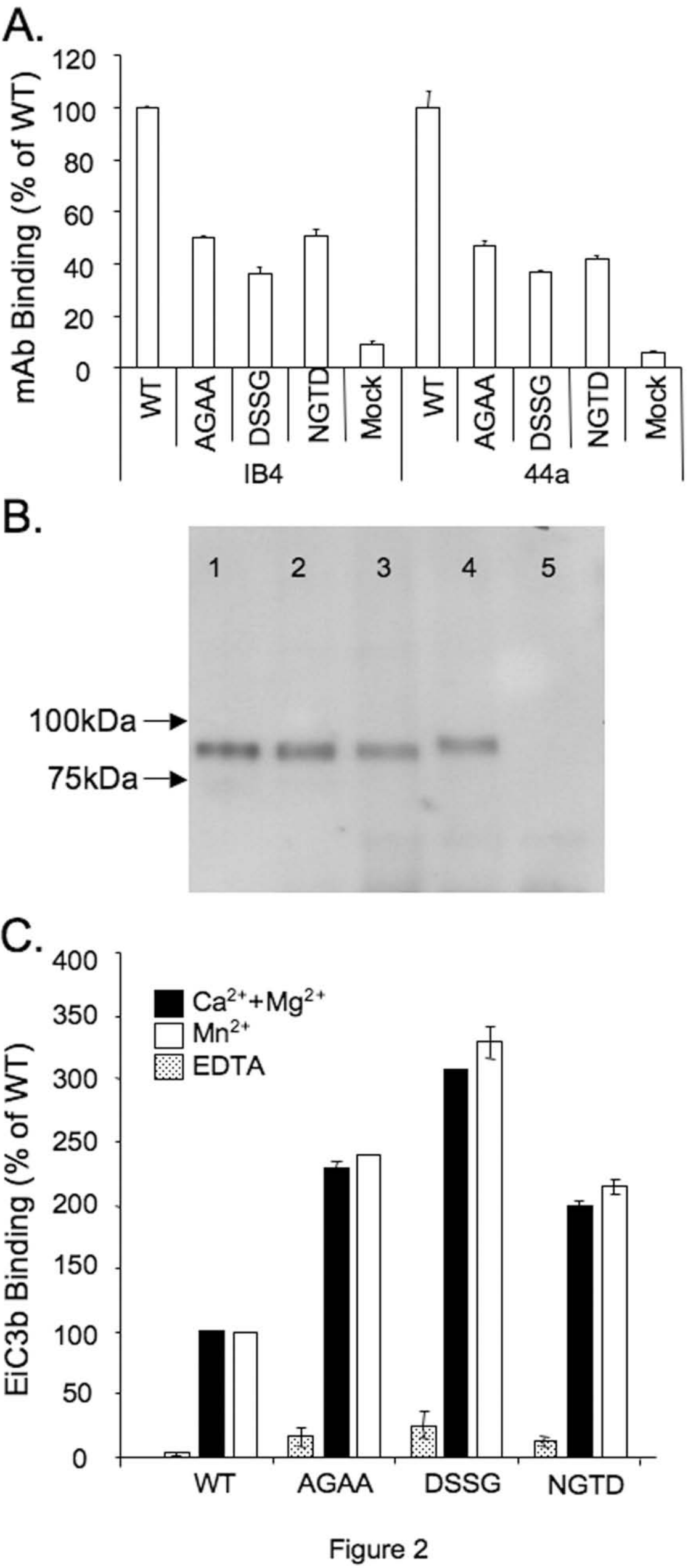
A.
mAb Binding (% of WT)
120
100
80
60
40
20
0
WT
AGAA
DSSG
NGTD
Mock
WT
AGAA
DSSG
NGTD
Mock
IB4
44a
B.
1
2
3
4
5
100kDa
75kDa
C.
EiC3b Binding (% of WT)
400
350
300
250
200
150
100
50
0
Ca2+ +Mg2+
Mn2+
EDTA
WT
AGAA
DSSG
NGTD

Figure 2

A.

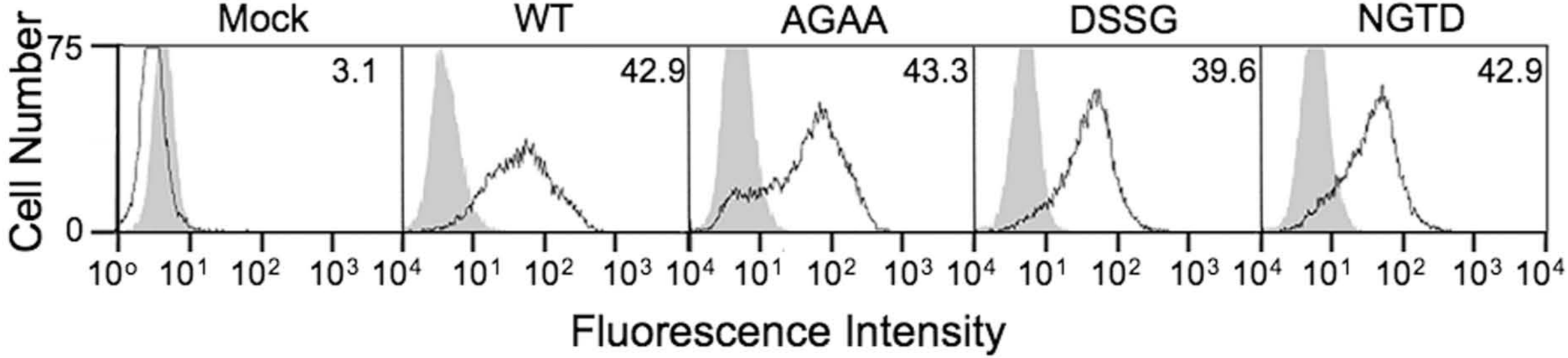
Mock
WT
AGAA
DSSG
NGTD
3.1
42.9
43.3
39.6
42.9
Cell Number
75
0
10^0 10^1 10^2 10^3 10^4
Fluorescence Intensity

B.

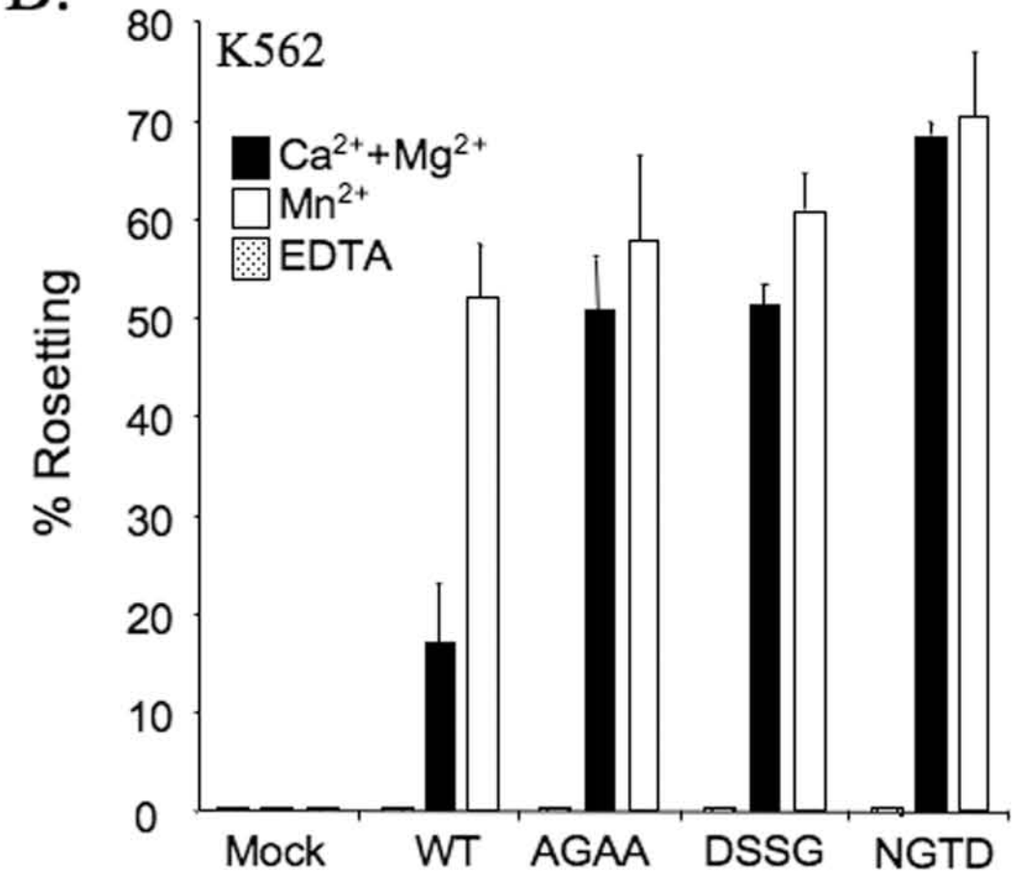
K562
$Ca^{2+}+Mg^{2+}$
Mn^{2+}
EDTA
% Rosetting
80
70
60
50
40
30
20
10
0
Mock
WT
AGAA
DSSG
NGTD

C.

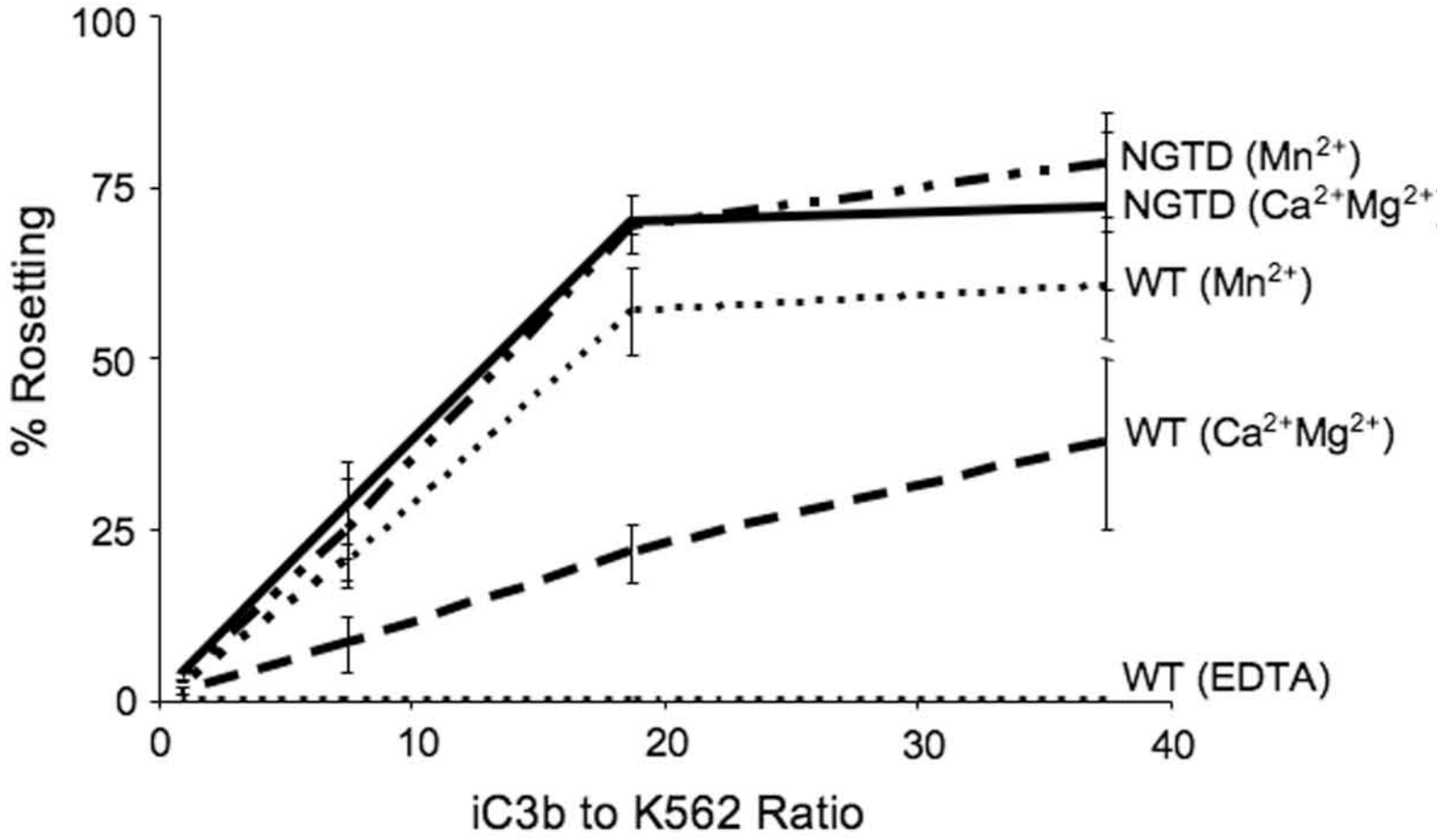
% Rosetting
100
75
50
25
0
0
10
20
30
40
iC3b to K562 Ratio
NGTD (Mn^{2+})
NGTD ($Ca^{2+}Mg^{2+}$)
WT (Mn^{2+})
WT ($Ca^{2+}Mg^{2+}$)
WT (EDTA)

Figure 3

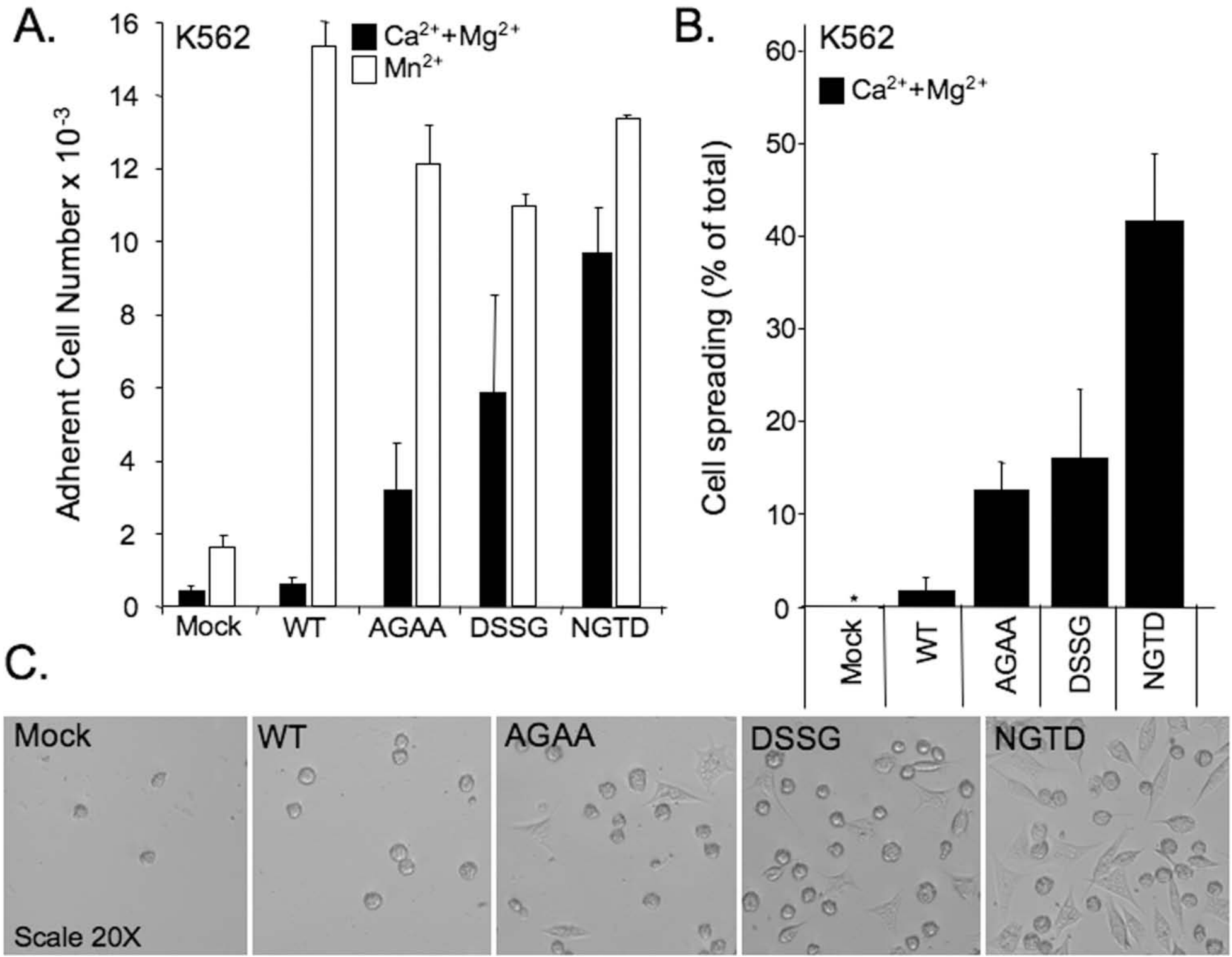
A.
K562
Ca2+ + Mg2+
Mn2+
Adherent Cell Number x 10-3
16
14
12
10
8
6
4
2
0
Mock
WT
AGAA
DSSG
NGTD
B.
K562
Ca2+ + Mg2+
Cell spreading (% of total)
60
50
40
30
20
10
0
*
Mock
WT
AGAA
DSSG
NGTD
C.
Mock
WT
AGAA
DSSG
NGTD
Scale 20X

Figure 4

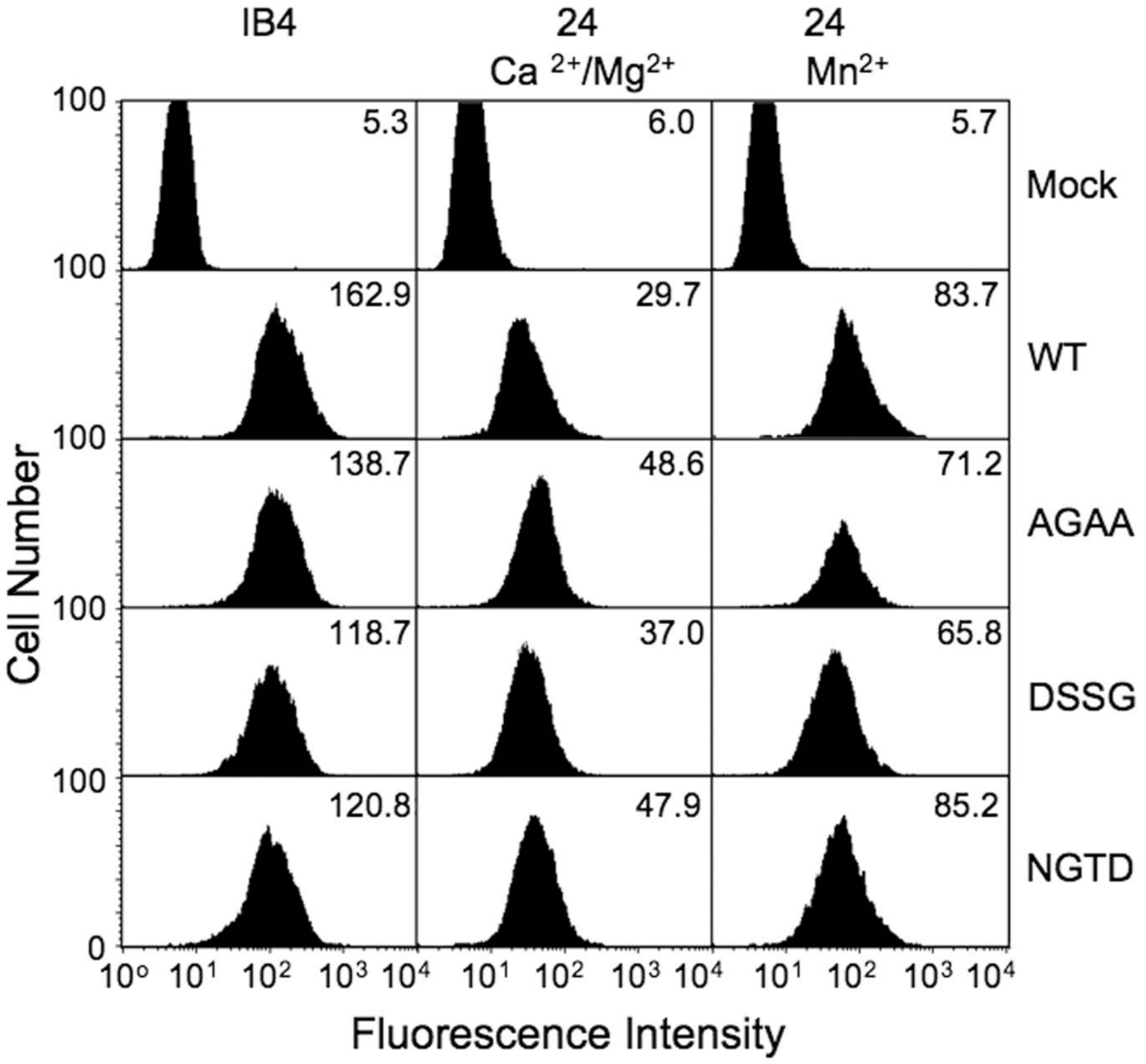
IB4
24
Ca 2+/Mg2+
24
Mn2+
Mock
WT
AGAA
DSSG
NGTD
5.3
6.0
5.7
162.9
29.7
83.7
138.7
48.6
71.2
118.7
37.0
65.8
120.8
47.9
85.2
100
100
100
100
0
Cell Number
10o 101 102 103 104
101 102 103 104
101 102 103 104
Fluorescence Intensity

Figure 5

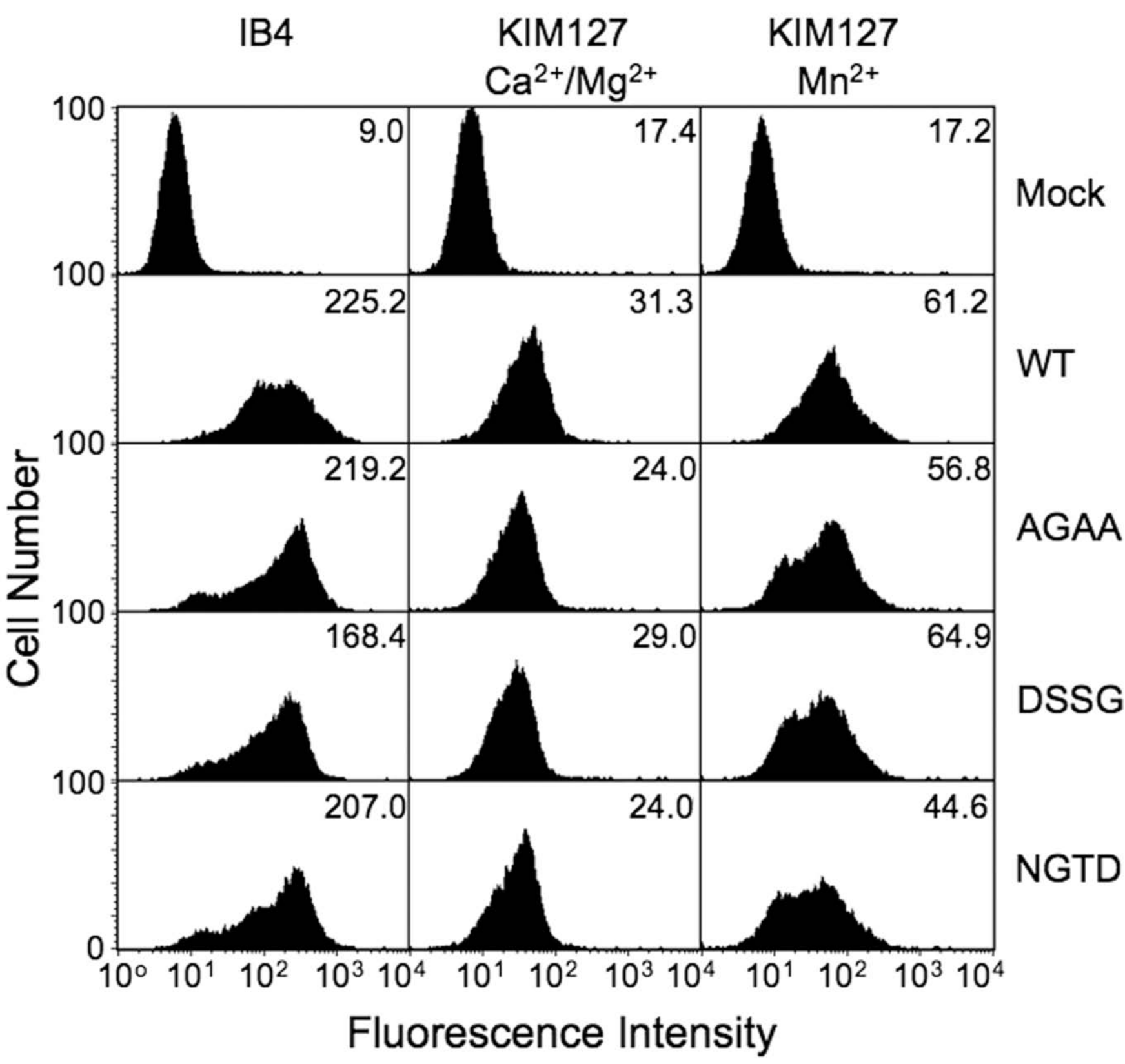
IB4
KIM127
Ca2+/Mg2+
KIM127
Mn2+
Mock
WT
AGAA
DSSG
NGTD
9.0
17.4
17.2
225.2
31.3
61.2
219.2
24.0
56.8
168.4
29.0
64.9
207.0
24.0
44.6
100
100
100
100
100
0
Cell Number
10o 101 102 103 104
101 102 103 104
101 102 103 104
Fluorescence Intensity

Figure 6

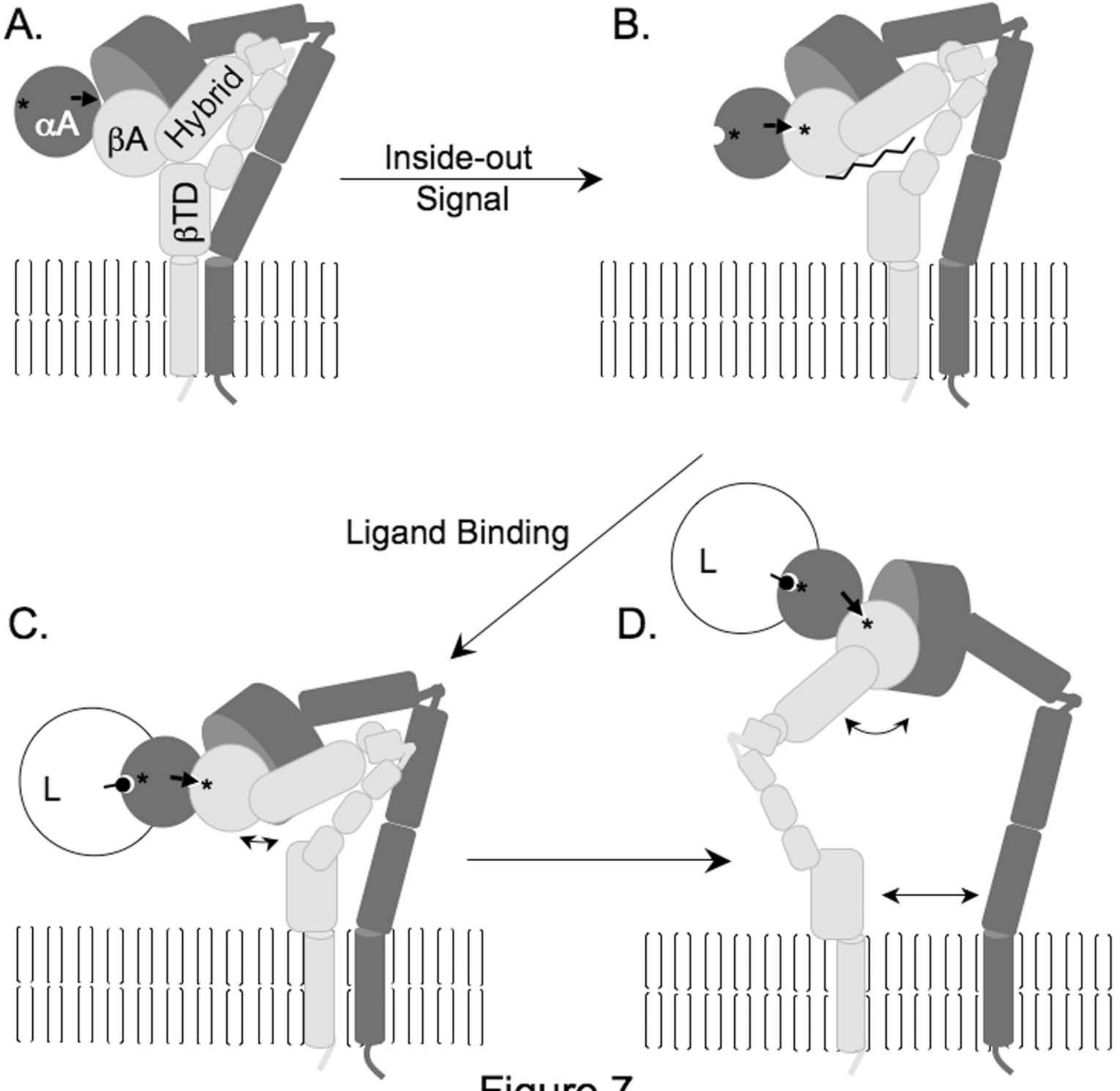

Figure 7